JOURNAL OF AIRCRAFT
Vol. 42, No. 1, January–February 2005

Incorporation of Aircraft Performance Considerations in Inverse Airfoil Design

Jeffrey K. Jepson* and Ashok Gopalarathnam†
North Carolina State University, Raleigh, North Carolina 27695-7910

Although significant advances have been made in inverse airfoil design methodology, the tailoring of an airfoil to maximize one or more aircraft performance parameters still involves cycling between airfoil design and aircraft performance computations. A design formulation is presented that incorporates aircraft performance considerations in the inverse design of low-speed laminar-flow airfoils for piston engine driven propeller-powered airplanes. Two aircraft performance parameters are considered: level-flight maximum speed and maximum range. It is shown that the lift coefficient for the lower and upper corners of the airfoil low-drag range can be appropriately adjusted to tailor the airfoil for these two aircraft performance parameters. The design problem is posed as a part of a multidimensional Newton iteration in an existing conformal-mapping based inverse design code, PROFOIL. This formulation automatically adjusts the lift coefficients for the corners of the low-drag range as required for the airfoil–aircraft matching. The design formulation also has the capability to handle a constraint on the stall speed by automatically adjusting the wing area to account for changes to the airfoil maximum lift coefficient. Two examples are presented to illustrate the process for a general aviation aircraft, and the results are validated by comparison with results from postdesign aircraft performance computations.

Nomenclature

AR	=	wing aspect ratio
b	=	wing span
C_D	=	aircraft or wing drag coefficient based on S_w
C_d	=	airfoil drag coefficient based on chord
C_L	=	aircraft or wing lift coefficient based on S_w
C_l	=	airfoil lift coefficient based on chord
C_l^*	=	design lift coefficient for a segment on the airfoil
C_m	=	airfoil pitching moment coefficient about the quarter-chord location
e	=	Oswald's efficiency factor
H_{12}	=	boundary-layer shape factor
M	=	Mach number
n	=	laminar boundary-layer transition amplification factor
P_{av}	=	power available
P_{req}	=	power required
R	=	aircraft range
Re	=	Reynolds number
S	=	area
V	=	aircraft velocity
W	=	aircraft weight
W_e	=	aircraft weight without fuel
W_f	=	aircraft weight with fuel
α^*	=	design angle of attack for a segment on the airfoil
α	=	angle of attack
η_p	=	propeller efficiency
ρ	=	density

Subscripts

f	=	fuselage and other components of aircraft except wing
i	=	induced
max	=	maximum
min	=	minimum
p	=	profile
stall	=	stall
w	=	wing

Superscripts

low	=	lower corner of the airfoil low-drag range
up	=	upper corner of the airfoil low-drag range

Introduction

THE objective of inverse airfoil design is to determine the shape of the airfoil that satisfices desired aerodynamic and geometric specifications. Under this traditional classification, inverse airfoil design methods have progressed significantly over the past several decades. The first pioneering methods (such as those by Mangler[1] and by Lighthill[2]) allowed for the prescription of the desired inviscid velocity distribution at a single angle of attack. Since then, inverse methods have steadily progressed to include multipoint velocity specifications,[3] single-point boundary-layer specifications,[4] multipoint velocity and boundary-layer specifications on single-element[5,6] and multi-element airfoils,[7] and specification of the laminar-to-turbulent transition curves[8] on the upper and lower surfaces of airfoils.

The benefit of the use of inverse methods that allow for prescription of the desired aerodynamics as an alternative to direct design via repeated geometry modifications is that the aerodynamics are more closely connected to the performance of the final system for which the airfoil is being designed. Recent work by Gopalarathnam and Selig[9] and Jepson and Gopalarathnam[8] illustrate the power of inverse approaches in the design of low-speed natural laminar flow (NLF) airfoils by showing how it is possible to control reliably the C_l values for the upper and lower corners of the low-drag range (LDR or drag bucket) by appropriate specification of the velocity and boundary-layer properties on different segments of the airfoil, along with the design lift coefficients and Reynolds numbers for the segments. By alteration of the chordwise locations and extents of these segments, it is possible to adjust the extents of the favorable pressure gradients on the upper and lower surfaces of the airfoil, thus controlling the extents of laminar flow and the resulting C_d at

Presented as Paper 2003-3499 at the Incorporation of Aircraft Performance Considerations in Inverse Airfoil Design, Orlando, FL, 23–26 June 2003; received 22 September 2003; revision received 9 February 2004; accepted for publication 10 February 2004.

*Graduate Research Assistant, Department of Mechanical and Aerospace Engineering, Box 7910; jkjepson@eos.ncsu.edu. Student Member AIAA.

†Assistant Professor, Department of Mechanical and Aerospace Engineering, Box 7910; ashok_g@ncsu.edu. Member AIAA.

the design conditions. With these capabilities, modern inverse methods allow for easy generation of families of airfoils with systematic changes to the lift, drag, and pitching moment characteristics. The most appropriate airfoil for a desired aircraft (or other application) can then be selected from among the airfoils in these families.

The process of tailoring an airfoil for an aircraft, therefore, typically involves cycling through airfoil design and aircraft performance simulations. The results of such performance simulations enable the examination of the tradeoffs involved in the choices of the different airfoil design parameters such as the C_l values for the upper and lower corners of the LDR. This process of selection of the most suitable airfoil candidate for an aircraft can be made considerably easier by the use of a figure-of-merit approach[10] for airfoil–aircraft design integration, or by the use of closed-form analytical expressions for the ideal C_l values for the LDR upper and lower corners, such as those derived by Gopalarathnam and McAvoy[11] for piston-propeller powered aircraft with constant values of the propeller efficiency and engine specific fuel consumption (SFC).

In spite of these improvements, the process of the tailoring of airfoils for an aircraft still relies on numerous postdesign aircraft performance simulations. For this reason, the objective of the research described in this article was to develop an approach that allows for the incorporation of aircraft performance considerations at the outset, during the inverse airfoil design process. The two aircraft performance parameters considered in this work are aircraft level-flight maximum speed and maximum range. Such an advancement was aimed at achievement of the next level of sophistication in inverse airfoil design technology, as a result of which inputs to inverse airfoil design can be expanded beyond the desired airfoil aerodynamics to include characteristics of the intended aircraft application such as wing area, wingspan, fuselage drag, and engine power. Overall design cycle time can also be considerably reduced by the use of such a method.

The following section provides an overview of the methodology for the inclusion of aircraft performance considerations in inverse airfoil design. A detailed description of the formulation used to tailor the airfoil for level-flight maximum speed $V_{\max}$ and maximum range $R_{\max}$ is then shown. A description of the analysis tools used for validation of the results from the design method is then presented. Finally, examples are presented to illustrate the capabilities of the method.

Overview of the Design Formulation

To present an overview of the formulation, the drag polar of a representative NLF airfoil, shown in Fig. 1, is considered. For the design formulation presented in this article, it is assumed that the airfoil has no camber-changing cruise flaps. This polar was obtained by analysis of the airfoil at a constant $Re\sqrt{(C_l)}$ to take into consideration the changes in Reynolds number as a result of changes in airspeed associated with variations in the operating C_l for an aircraft in rectilinear flight. The C_l values for the upper and lower corners of the LDR, C_l^{up} and C_l^{low}, are marked in Fig. 1. Desired values of these lift coefficients for given extents of laminar flow are easily achieved during inverse design by changes to airfoil camber and thickness, as illustrated in Ref. 9. It was also shown in Refs. 9 and 11 that for changes to the airfoil camber and thickness with a given extent of laminar flow, the points on the polar corresponding to C_l^{up} and C_l^{low} move along a locus trajectory that is close to a straight line in the C_d–C_l plot. This low-drag curve is marked in Fig. 1. It is not clear at the airfoil design stage, however, as to what are the most suitable values of the C_l^{up} and C_l^{low} to tailor the airfoil to suit a given aircraft to maximize the performance of the aircraft.

Two aircraft performance parameters were considered in this study: level-flight maximum speed $V_{\max}$ and maximum range $R_{\max}$. Earlier work[11] demonstrated the suitability of the use of the two lift coefficients C_l^{up} and C_l^{low} as design variables to tailor an NLF airfoil for maximization of these two aircraft performance parameters. When an airfoil is tailored for these performance parameters for a given aircraft, the following questions can be posed: 1) What is the best possible value of C_l^{low} to tailor the airfoil to achieve the highest possible $V_{\max}$ without sacrificing low-speed performance? 2) What is the best possible value of C_l^{up} to tailor the airfoil for the maximum-range condition without unnecessary penalties at the high-speed conditions? The objective was to formulate the airfoil design problem to achieve this airfoil–aircraft matching from the outset during the inverse airfoil design stages.

The following three paragraphs provide an overview of how an airfoil can be tailored for the $V_{\max}$ or $R_{\max}$ conditions of an aircraft during the inverse design process. For this purpose, a hypothetical aircraft with given wing planform geometry, fuselage drag, and power characteristics is considered. A baseline airfoil is assumed as the initial choice for the wing, and this subsection shows how the camber of the baseline airfoil can be adjusted for tailoring the airfoil for either the $V_{\max}$ or $R_{\max}$ flight conditions.

Figure 2a shows the drag polars for the starting, or baseline, airfoil and for the airfoil tailored for $V_{\max}$. Also shown in Fig. 2a are the low-drag curve and the locations of C_l^{low} for both airfoils. It is seen that, in this example, the tailored airfoil has a lower value of C_l^{low} than does the baseline airfoil. The full-power aircraft rate-of-climb (ROC) variations for both airfoils are shown in Fig. 2b, along with the points corresponding to C_l^{low} for the two airfoils. Note that the velocity corresponding to zero ROC is $V_{\max}$, then, it is seen that by lowering the C_l^{low} of the baseline airfoil, the value of $V_{\max}$ has increased. Not only is the aircraft $V_{\max}$ with the baseline airfoil less than with the tailored airfoil, but it also occurs at a C_l that lies outside of the drag

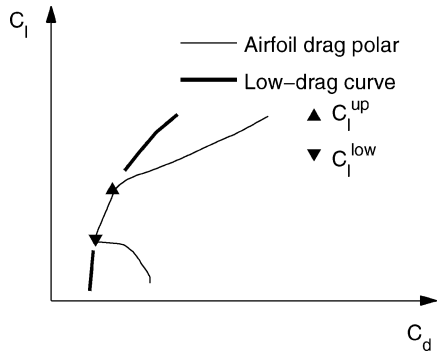

Fig. 1 Airfoil drag polar.

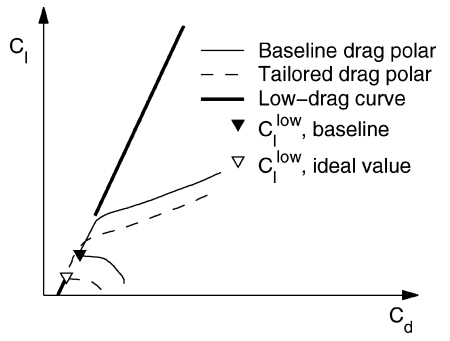

a) Drag polars for the baseline airfoil and the airfoil tailored for $V_{\max}$

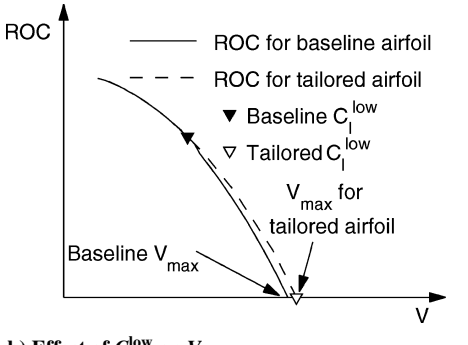

b) Effect of C_l^{low} on $V_{\max}$

Fig. 2 Airfoil tailoring for $V_{\max}$.

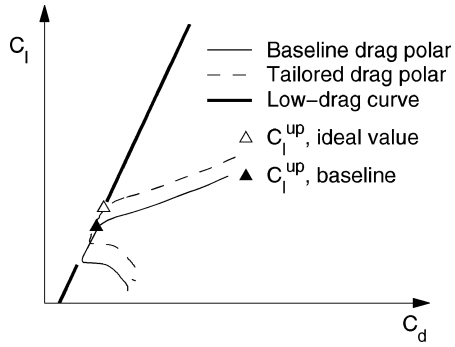

a) Drag polars for the baseline airfoil and the airfoil tailored for R_{max}

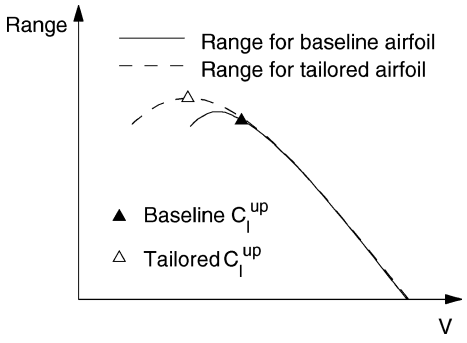

b) Effect of C_l^{up} on R_{max}

Fig. 3 Airfoil tailoring for R_{max}.

bucket of the baseline airfoil. In addition, the C_l^{low} of the tailored airfoil is the C_l value that corresponds to zero ROC. Therefore, to tailor an airfoil to maximize V_{max}, the drag bucket should be placed in such a way that the C_l^{low} corresponds to the condition of zero ROC. This illustration provides useful guidelines for incorporation of the airfoil–aircraft tailoring for the V_{max} condition in the inverse design process. A Newton iteration procedure can be used to adjust the design parameters that control the C_l^{low} until C_l^{low} corresponds to the V_{max} condition, that is, until ROC $= 0$ at $C_l = C_l^{low}$.

The drag polars for the baseline airfoil and the airfoil tailored for R_{max} are shown in Fig. 3a. Also shown are the low-drag curve and the values of C_l^{up} for both airfoils. As Fig. 3 shows, in this instance, the C_l^{up} for the tailored airfoil is higher than that for the baseline airfoil. Figure 3b shows the variation of aircraft range R with velocity V for the two airfoils along with the points corresponding to C_l^{up} for the two airfoils. Note that the aircraft has a greater R_{max} with the tailored airfoil than with the baseline airfoil Furthermore, the R_{max} with the baseline airfoil occurs during operation outside of the drag bucket. The ideal value of C_l^{up} is found by determination of the value of C_l along the low-drag curve that gives the maximum value of R_{max}. The tailored airfoil will have a C_l^{up} that corresponds to this ideal value of C_l^{up}. This matching can be achieved in the inverse design framework by the use of Newton iteration to adjust the design variables that affect C_l^{up} until the difference between C_l^{up} and the ideal value of C_l^{up} is brought to zero.

Design Formulation

To incorporate aircraft performance considerations in inverse airfoil design, the inverse airfoil design method PROFOIL[5,6] was adapted. This section first briefly describes some of the main features of PROFOIL and then discusses the development of the design formulation that incorporates the two aircraft performance considerations (level-flight maximum speed V_{max} and maximum range R_{max}) in the PROFOIL code.

Description of the PROFOIL Code

PROFOIL[5,6] is a multipoint inverse design method based on conformal mapping. In the method, the airfoil is divided into a finite number of segments, each having a design angle of attack α^* that is measured relative to α_{0l}. For each segment, the velocity distribution over the segment at $\alpha = \alpha^*$ is prescribed and can either be constant (as in the Eppler method, see Ref. 3) or can have a nonlinear variation by the use of a cubic-spline description.[6] Specification of α^* is equivalent to specification of a design value of C_l, referred to as C_l^* because α^* is measured relative to α_{01} and the slope of the lift curve is approximately 2π per radian. In other words, the design lift coefficient for any segment is related to the segment α^* (in degrees) by Eq. (1):

$$C_l^* \approx 0.1 \times \alpha^* \tag{1}$$

PROFOIL can also solve for the boundary-layer development along the upper and lower surfaces of the airfoil at a specified C_l by the use of a direct integral method. For a given airfoil, PROFOIL uses the inviscid velocity distribution to calculate boundary-layer properties such as the shape factor H_{12} and the transition amplification factor n. Because this boundary-layer calculation is used in conjunction with the rapid, interactive design environment in PROFOIL, no viscous–inviscid interaction is used. In other words, the inviscid pressure distribution is not adjusted to account for the effects of the boundary-layer displacement thickness. The n development is calculated using Drela's approximate e^n method described in Refs. 12 and 13.

In the current approach to airfoil–aircraft matching, there is a need to determine the airfoil C_d at specified values of C_l within the drag bucket several times during the inverse design process. A procedure was developed for determination of an approximate but rapid estimate for the airfoil C_d within the PROFOIL code. The assumption in the approximate method is that the pressure-drag contributions can be neglected when airfoil C_d is estimated for C_l values that lie within or at the corners of the LDR. In the approach developed in this research, the airfoil C_d is computed at a given C_l first by the use of the airfoil inviscid velocity distribution, along with the direct integral boundary-layer method in PROFOIL to determine the laminar boundary-layer transition locations on the upper and lower surfaces. In the current work, transition is assumed to occur when n reaches a user-specified critical value, n_{crit}. This assumption is valid for flows where transition is caused by the amplification of Tollmien–Schlichting waves. For those cases in which the laminar boundary layer separates before n reaches n_{crit}, transition to turbulence is assumed to occur at the point of laminar separation. This assumption is reasonable for NLF airfoils that have small separation bubbles. The skin-friction drag coefficient is then estimated by the use of flat-plate boundary-layer equations from Ref. 14 for the known extents of laminar and turbulent boundary layers on both surfaces of the airfoil.

Figure 4 shows a comparison between the skin-friction drag calculated with this approximate approach and the total airfoil drag obtained from XFOIL analysis. Note that the skin-friction drag closely corresponds to the total drag at C_l values within the drag bucket. This approximate method of determination of the airfoil C_d was developed to obtain rapid estimates suitable for the potentially large

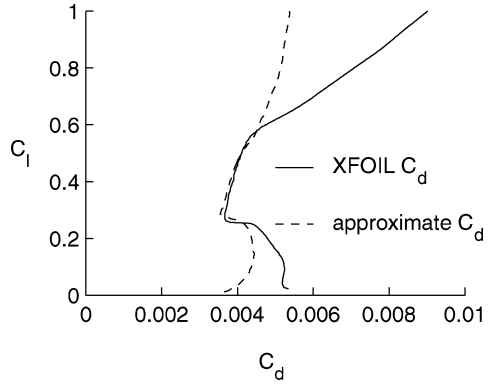

Fig. 4 Comparison between skin-friction drag and total drag for the baseline airfoil at $Re\sqrt{(C_l)} = 3.42 \times 10^6$.

number of C_d evaluations that could be required during inverse design.

One of the main features of PROFOIL is the multidimensional Newton iteration scheme that allows for the prescription of several aerodynamic and geometric characteristics. This multidimensional Newton iteration scheme is utilized as a key feature in the current work to incorporate the aircraft $V_{\max}$ and $R_{\max}$ design considerations. In this scheme, control over some of the parameters used in conformal mapping is given up to achieve the desired specifications. These parameters are altered via Newton iteration until the desired specifications are satisfied. The matrix equation shown in Eq. (2) is solved at each step of the Newton iteration:

$$\boldsymbol{J} \cdot \delta \boldsymbol{x} = -\boldsymbol{F} \tag{2}$$

In this matrix equation, $\boldsymbol{F}$ is the vector containing the residuals of the functions to be zeroed, $\boldsymbol{J}$ is the $n \times n$ Jacobian matrix that contains the gradient information, and $\delta \boldsymbol{x}$ contains the corrections to the design variables to make $\boldsymbol{F}$ approach zero. For each step of the iteration, $\delta \boldsymbol{x}$ is found and applied to the design variables. This process is continued until the desired specifications are achieved to within a given tolerance.

Airfoil Tailoring for $V_{\max}$

As illustrated in Fig. 2, an airfoil tailored for the aircraft $V_{\max}$ condition will have ROC = 0 at the flight speed corresponding to C_l^{low}. To examine how to incorporate this design statement in the inverse-design Newton iteration structure, it is necessary to examine the contribution of the airfoil C_d to the aircraft ROC. For airfoils that are designed by posing the inverse design problem as shown in Ref. 9, the C_l^{low} is the design C_l of the lower surface. The approximate airfoil C_d is then computed at this C_l with the skin-friction C_d estimate described in the preceding subsection.

With the assumptions that the aircraft $C_L = C_l^{\text{low}}$ and that the wing profile drag coefficient is equal to the airfoil C_d, the aircraft C_D can be determined by addition of the parasite-drag contribution of the fuselage and other components and wing C_{D_i} to the wing profile drag coefficient:

$$C_D = C_d + C_{Df} S_f / S_w + C_L^2 \big/ \pi e \mathrm{AR} \tag{3}$$

At the aircraft velocity V corresponding to C_L, the resulting aircraft drag, power required for level flight, and rate of climb can then be determined.

$$D = \frac{1}{2}\rho V^2 (C_d S_w + C_{Df} S_f) + \frac{2W^2}{\pi b^2 e \rho V^2} \tag{4}$$

$$P_{\text{req}} = \frac{1}{2}\rho V^3 (C_d S_w + C_{Df} S_f) + \frac{2W^2}{\pi b^2 e \rho V} \tag{5}$$

$$\text{ROC} = \eta_p P_{\text{av}} - P_{\text{req}} \tag{6}$$

The elements of the residual and the Jacobian for the Newton equation for the $V_{\max}$ tailoring can be then computed:

$$F = (\text{ROC})_{C_l^{\text{low}}} - 0.0 \tag{7}$$

$$J = \frac{\partial (\text{ROC})_{C_l^{\text{low}}}}{\partial \alpha^*} \tag{8}$$

Thus, when the design problem is posed as a part of the Newton iteration framework, the inverse method can be used to determine the ideal value of C_l^{low} for a given aircraft and determine the corresponding airfoil shape.

Airfoil Tailoring for $R_{\max}$

An airfoil tailored for the maximum-range flight condition needs to have the C_l^{up} equal to the ideal value of C_l^{up}, as shown earlier in Fig. 3. The equation for range R at any given C_l is the well-known Bréguet range equation:

$$R = \frac{\eta}{\text{SFC}} \frac{C_L}{C_D} \int_{W_e}^{W_f} \frac{\mathrm{d}W}{W} \tag{9}$$

For this airfoil design problem, the equations for the elements of the residual and the Jacobian for this Newton equation are

$$F = C_l^{\text{up}} - \left(C_l^{\text{up}}\right)_{\text{ideal}} \tag{10}$$

$$J = \frac{\partial C_l^{\text{up}}}{\partial \alpha^*} \tag{11}$$

The aircraft C_D is computed with Eq. (3), for which the airfoil C_d is estimated by the use of the approximate method described earlier. In this case also, the pressure drag contributions of the airfoil are assumed to be small because the airfoil is operating within the drag bucket.

The determination of the value of C_l^{up} within the PROFOIL code is not straightforward. Unlike for the lower surface, the values of α^* for the segments on the upper surface vary significantly from the leading edge to the trailing edge.[9] For this reason, the C_l^{up} for the initial airfoil is first determined by generation of a drag polar via XFOIL and is provided as an input to the PROFOIL code. Because the slope of the airfoil lift curve is approximately 0.1 per degree, a change of $\Delta\alpha^*$ to the α^* values for the upper-surface segments results in a predictable change of $0.1\Delta\alpha^*$ to the airfoil C_l^{up}. This predictable relationship is used so that anytime the α^* values for the upper-surface segments change by $\Delta\alpha^*$ during the Newton iteration process, the current value of C_l^{up} is adjusted by $0.1\Delta\alpha^*$. For the determination of $(C_l^{\text{up}})_{\text{ideal}}$, a linearized approximation to the equation for the low-drag curve is obtained by use of finite differencing to determine the change in airfoil skin-friction C_d for a given change in the C_l of the airfoil. The assumption in this approximation is that the slope of the low-drag curve in the vicinity of C_l^{up} is the same as the slope of the airfoil C_d–C_l curve within the LDR at C_l^{up}. At every step of the Newton iteration, this linearized equation for the low-drag curve is computed and used in the code to determine the ideal C_l^{up}.

The use of such approximations in C_l and C_d in the design formulation enables rapid design via the Newton iteration process. Note that the objectives in the design formulation are only to determine the ideal values of C_l^{low} and C_l^{up} and not to predict the resulting values of $V_{\max}$ and $R_{\max}$. For these objectives, the approximations are not only valid, but also enable rapid, interactive design.

Analysis Tools for Validation

This section describes the tools and the methodology that were used to validate the results obtained via the PROFOIL code. The first step in the validation approach was to analyze the converged airfoil with the XFOIL code[12] to calculate the drag polar of the airfoil to take into consideration both the pressure and skin-friction contributions to the airfoil C_d.

Once the airfoil drag polar was calculated, the WINGS code[11] was used to calculate the trimmed induced and profile drag of the lifting surfaces of the aircraft. WINGS is a vortex lattice code that can handle multiple lifting surfaces. The code reads in the XFOIL α-C_l-C_d-C_m polar output files to allow for the use of the airfoil drag polar and pitching moment curves for various sections along the wing and horizontal tail. In the analysis with WINGS, the incidence of the horizontal tail at each angle of attack was adjusted to trim the aircraft, that is, to set $C_{M\text{c.g.}} = 0.0$. This ensured that the aircraft performance estimates took into account the trimmed drag contributions associated with changes to the wing airfoil $C_{Mc/4}$ that accompany changes to the airfoil camber.

After the total drag of the aircraft was calculated, the performance of the aircraft was calculated by the use of PERF.[11] PERF is an aircraft performance simulation code that uses the equations discussed in the preceding section along with the drag output from the WINGS code to calculate the aircraft rate of climb and range at each angle of

attack. This postdesign approach was used to generate all of the performance plots in the demonstration section to validate the results obtained from the inverse design method.

Aircraft Specification

This section presents the relevant details of a hypothetical general aviation aircraft used as an example application in the rest of the article. The aircraft is a conventional, aft-tail configuration with a constant-speed propeller driven by a piston engine. The planview of the wing and tail of the aircraft is shown in Fig. 5.

Table 1 provides the relevant specifications for the aircraft. As shown, an equivalent parasite drag area ($C_{Df}S_f$) was assumed for the fuselage and all of the components of the airplane except the wing. The propeller efficiency was assumed to have the nonlinear variation with velocity shown in Fig. 6. The static margin for the hypothetical aircraft was assumed to be 15% of the wing mean aerodynamic chord. The wing area for this baseline configuration was assumed to be 9.1 m^2 and results in a flaps-down stall speed of 33.5 m/s in the landing configuration.

Table 1 Assumed geometry, drag, and power characteristics for the hypothetical general aviation airplane

Parameter	Value
Gross weight W	14,269 N (3,200 lbf)
Wing reference area S_w	9.10 m^2 (97.92 ft^2)
Wing aspect ratio AR	9.1
Equivalent parasite drag area of airplane minus wing $C_{Df}S_f$	0.1647 m^2 (1.772 ft^2)
Rated engine power P_{av}	261 kW (350 hp)
SFC	8.31×10^{-7} N/s/W (0.5 lbf/h/hp)
Fuel volume	341 liters (90 U.S. gal)
Target V_{stall} (landing configuration)	33.5 m/s (75.4 mph)

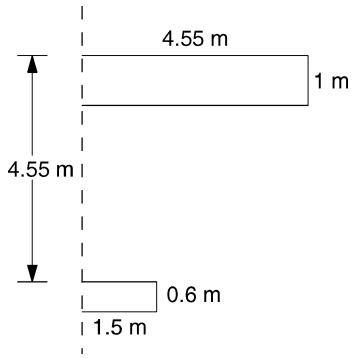

Fig. 5 Planview showing the right-side geometry of the wing and tail for hypothetical aircraft.

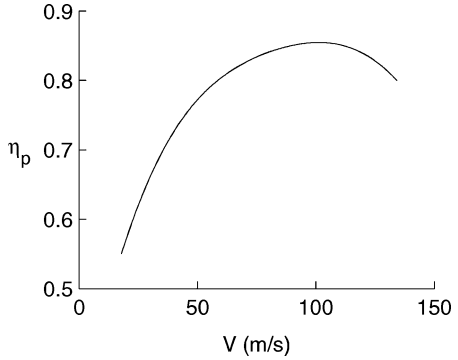

Fig. 6 Assumed propeller efficiency distribution.

Demonstration of the Method

For the demonstration of the method, a baseline unflapped NLF airfoil is used as an initial candidate wing section for the propeller-driven general aviation aircraft shown earlier in Fig. 5. This baseline airfoil was designed based on the methodology described in Ref. 9 for a reduced Reynolds number $Re\sqrt{(C_l)}$ of 3.42×10^6. This reduced Reynolds number corresponds to rectilinear flight at standard sea-level conditions for the aircraft. The airfoil was designed to support at least 50%c laminar flow on the upper and lower surfaces when operating in the LDR. The α^* for the lower surface was set at 2.5 deg, resulting in the lower-surface design C_l of 0.25. This specification resulted in a C_l^{low} of 0.25 for the drag polar at this reduced Reynolds number. The thickness-to-chord ratio was specified to be 14% and was achieved by iteration on the α^* values for the segments on the upper surface. As a result of these specifications, the C_l^{up} for this polar is 0.6.

Airfoil Tailoring for V_{max}

For tailoring the airfoil to suit the aircraft V_{max} condition, the α^* values of the lower-surface segments were adjusted with the Newton iteration scheme described earlier. The maximum thickness ratio was maintained at 14%. As a result, changes to the airfoil are similar to changes to the maximum camber. The geometry and inviscid velocity distributions for the baseline airfoil and the converged airfoil (labeled A) are shown in Fig. 7. Note that the converged airfoil has a lower camber as a result of satisfying the specifications. The drag polars from XFOIL analysis for the baseline and converged airfoils are shown in Fig. 8. It is seen that the C_l^{low} for the converged airfoil A is 0.15 and was determined by the method as an outcome of tailoring the airfoil for the V_{max} condition. The ROC curves for

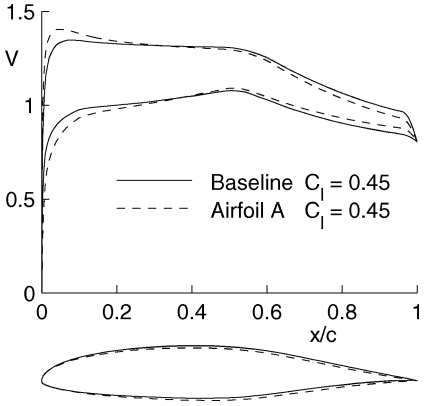

Fig. 7 Geometries and inviscid velocity distributions for the baseline airfoil and the converged airfoil A.

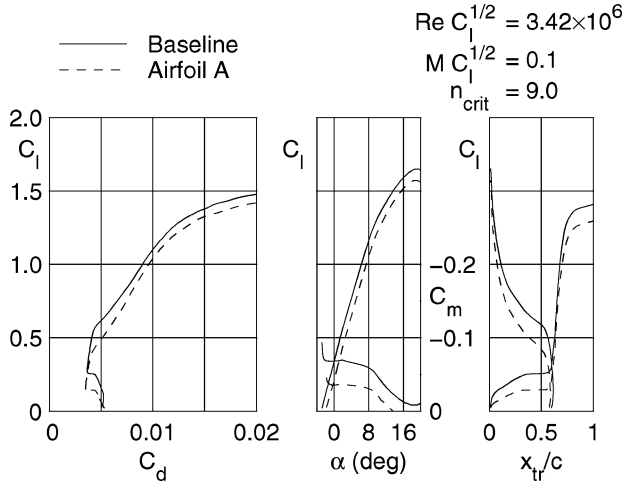

Fig. 8 Polars for the baseline airfoil and the converged airfoil A from XFOIL analysis.

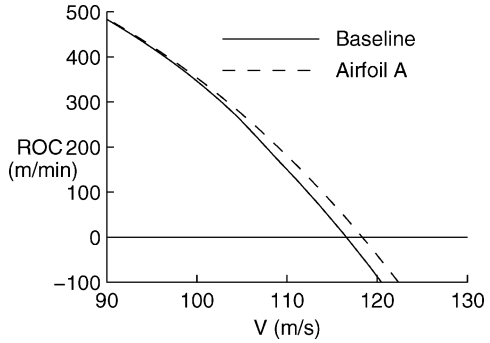

Fig. 9 Rate of climb curves with the baseline airfoil and the converged airfoil *A*.

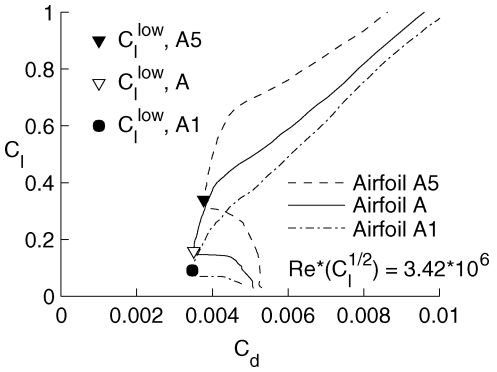

Fig. 10 Drag polars for airfoils *A*, *A*1, and *A*5.

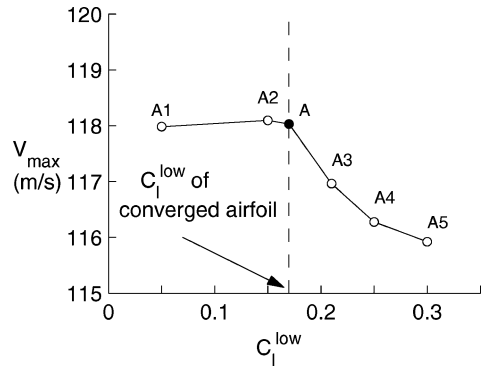

Fig. 11 V_{max} as a function of C_l^{low}.

the baseline and converged airfoils are shown in Fig. 9. As Fig. 9 shows, the converged airfoil has a higher V_{max}, as seen by the higher velocity at which ROC = 0 for the airfoil *A*.

Whereas the converged airfoil does indeed have a higher V_{max} than the baseline airfoil, it is not evident from the information in Figs. 7–9 that the airfoil *A* is necessarily the one that is ideally tailored for the V_{max} condition. To examine this situation, a family of airfoils with different values of C_l^{low} was designed around the airfoil *A*. Airfoils *A*1 and *A*2 were designed to have C_l^{low} less than 0.15, and airfoils A3–A6 were designed to have C_l^{low} greater than 0.15. The drag polars for airfoils *A*, *A*1, and *A*5 from XFOIL predictions are shown in Fig. 10. Also marked in Fig. 10 are the C_l^{low} values for the three airfoils. Figure 11 shows the variation of V_{max} as a function of C_l^{low} for the airfoils from the postdesign analysis. It is seen that as C_l^{low} is decreased from 0.3, the V_{max} increases progressively up to a value of C_l^{low} of 0.15, which corresponds to the C_l^{low} for the converged airfoil *A*. Any decrease in C_l^{low} beyond that for airfoil *A* results in a zero or small decrease in the V_{max}. The reason for this trend is that the airfoils *A*3–*A*6 have too high a C_l^{low} and the airfoils *A*1 and *A*2 have too low a C_l^{low} for the aircraft under consideration. The fact that airfoil *A* is ideally tailored for V_{max} is reinforced by examination

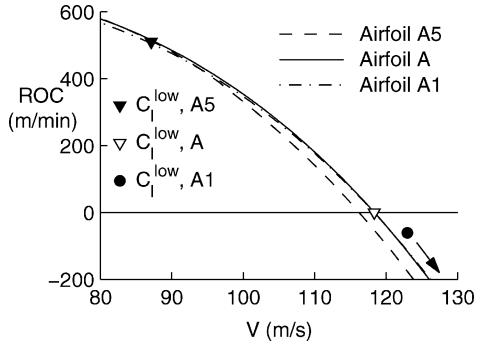

Fig. 12 Rate of climb curves with airfoils *A*, *A*1, and *A*5.

of Fig. 12, which shows the ROC curves for *A*, *A*1, and *A*5. It is seen that airfoil *A*5 has a lower V_{max} than that of airfoil *A*, whereas airfoil *A*1 does not have a higher V_{max}. Furthermore, the V_{max} for *A*5 occurs outside of the drag bucket. This postdesign study of the effect of camber on V_{max} demonstrates that the design formulation successfully tailors the airfoil for the V_{max} flight condition.

Airfoil Tailoring for V_{max} with Specified V_{stall}

In the preceding subsection, the airfoil tailoring for the V_{max} condition was done for a specified wing planform area ($S_w = 9.1$ m^2). Whereas the resulting tailored airfoil *A* has a lower C_l^{low} in comparison to the baseline airfoil, the $C_{l\max}$ of the airfoil *A* is also lower than that of the baseline, as seen from Fig. 8. In other words, the increase in V_{max} as a result of the tailoring is accompanied by an undesirable increase in the aircraft stall speed V_{stall} when the wing area is left unchanged. The stall speed with airfoil *A* can be made equal to that with the baseline airfoil if the wing area with airfoil *A* is increased in comparison to the baseline wing area. An increase in the wing area would, however, decrease the V_{max} achieved with the use of airfoil *A* as a result of increased wetted area. This effort to maintain a given V_{stall} during the airfoil tailoring process leads to the following two questions: 1) If the wing area is increased with the tailored airfoil *A*, will the decrease in V_{max} due to larger wing area outweigh the increase in V_{max} achieved with the reduced camber? 2) What is the ideal airfoil for the V_{max} condition when V_{stall} is maintained at a specified value by adjustment of the wing area appropriately with changes to airfoil $C_{l\max}$ that accompany changes to airfoil C_l^{low}?

To answer these questions, an option to adjust the wing area S_w to maintain a specified V_{stall} was incorporated in the Newton iteration for the V_{max}-tailoring process described earlier. In this study, the V_{stall} specification is made for the landing condition in which a part-span slotted flap is used to achieve an increase in the aircraft $C_{L\max}$. This option in the Newton iteration requires as input a relationship between airfoil C_l^{low} and aircraft $C_{L\max}$. For the family of airfoils with the same thickness ratio and laminar extents, but different cambers, the airfoil C_l^{low}-$C_{l\max}$ variation was obtained from XFOIL analysis of airfoils *A*1–*A*5 and is shown in Eq. (12). The C_l^{low}-$C_{L\max}$ relationship used in the current study is shown in Eq. (13), in which the $\Delta C_{L_{max}}$ is the increment assumed from the high-lift part-span slotted flap. For the current study, $\Delta C_{L_{max}}$ was assumed to be 0.65. With this C_l^{low}-$C_{L\max}$ relationship, the wing area S_w was adjusted in Eqs. (3–6) at every step of the Newton iteration, so that the stall speed was maintained at the specified value of 33.5 m/s (75.4 mph). The wingspan and aircraft weight were maintained constant; changes to the wing area resulted in proportional changes to the wing chord and, in turn, resulted in changes to the operating reduced Reynolds number $Re\sqrt{(C_l)}$. This change to the $Re\sqrt{(C_l)}$ was incorporated in the Newton iteration to take into account the changes to the development of the boundary-layer characteristics and the resulting effects on the transition location and the airfoil skin-friction C_d:

$$C_{l\max} = 0.59\left(C_l^{low}\right) + 1.49 \tag{12}$$

$$C_{L\max} = C_{l\max} + \Delta C_{L\max} = 0.59\left(C_l^{low}\right) + 1.49 + \Delta C_{L\max} \tag{13}$$

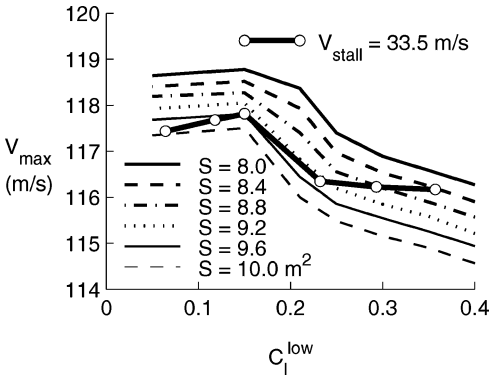

Fig. 13 V_{max} as a function of C_l^{low} for various values of S_w.

When starting with the baseline airfoil, tailoring for the V_{max} condition with a specified V_{stall} for the hypothetical general aviation aircraft resulted in an airfoil that was virtually identical to airfoil A with a C_l^{low} equal to 0.15. That is, the ideal airfoil for the V_{max} condition was found to be the same whether the wing area was left unchanged or whether the stall speed was maintained at a specified value during the tailoring process. When the stall speed is maintained unchanged, the Newton iteration process not only determines the ideal airfoil, but also the associated change in wing area. For the current problem, the wing area with the ideal airfoil A was found to be 9.3 m^2 to keep the stall speed at the specified value of 33.5 m/s (75.4 mph). If the wing area had been left unchanged at the baseline value of 9.1 m^2, the stall speed would have increased to 33.9 m/s (76.2 mph).

In an effort to better understand the reason for these results, a postdesign analysis study was performed with airfoils $A1$–$A5$ to study the effect of C_l^{low} on V_{max} for a range of wing areas from 8.0 to 10 m^2. The wingspan and aircraft weight were kept constant and the $Re\sqrt{(C_l)}$ was adjusted to take into account changes to the wing chord. As with the postdesign study performed earlier for the single wing area, the airfoil C_d estimate from XFOIL analysis includes both pressure and skin-friction drag contributions, and the aircraft induced-drag estimate from WINGS analysis includes the trim considerations. Figure 13 shows the results along with the points corresponding to a constant V_{stall} of 33.5 m/s (75.4 mph). The results for the constant V_{stall} curve clearly show that the ideal airfoil for the V_{max} condition is the one for which C_l^{low} is 0.15.

This study provides the answers to the two questions posed earlier in this section: 1) The negative effect of the wing-area increase on V_{max} does not outweigh the increase in V_{max} that results from tailoring an airfoil for this flight condition. 2) The ideal airfoil for the V_{max} condition is the same whether the wing area is kept unchanged or whether the wing area is adjusted to maintain a specified stall speed. Although these results are specific to the example airfoil family and aircraft used for illustration, the general trends may be applicable to a wide range of general aviation aircraft. More importantly, the Newton iteration inverse design approach presented is general and is applicable for tailoring of NLF airfoils for a wide range of aircraft.

Airfoil Tailoring for R_{max}

For tailoring the airfoil to suit the aircraft R_{max} condition, the α^* values of the lower-surface segments were varied with the Newton iteration scheme described earlier. The maximum thickness ratio was maintained at 14%. Although it is the upper corner of the polar that directly controls the maximum range, variation of the lower-surface α^* and maintenance of the maximum thickness specification is essentially equivalent to a variation of the C_l^{up}. As a result, changes to the airfoil are similar to changes to the maximum camber. The geometry and inviscid velocity distributions for the baseline airfoil and the converged airfoil (labeled B) are shown in Fig. 14. It is seen that the converged airfoil B has a higher camber as a result of satisfying the Newton equation in Eq. (10). The drag polars for the baseline and converged airfoil B are shown in Fig. 15. It is seen

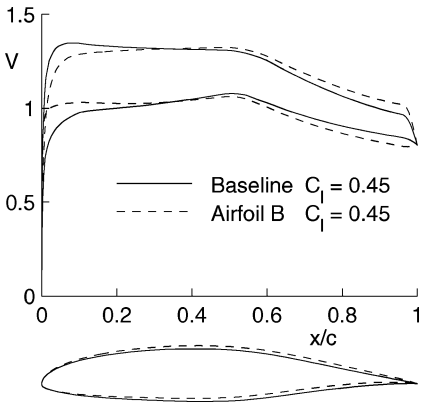

Fig. 14 Geometries and inviscid velocity distributions for the baseline airfoil and the converged airfoil B.

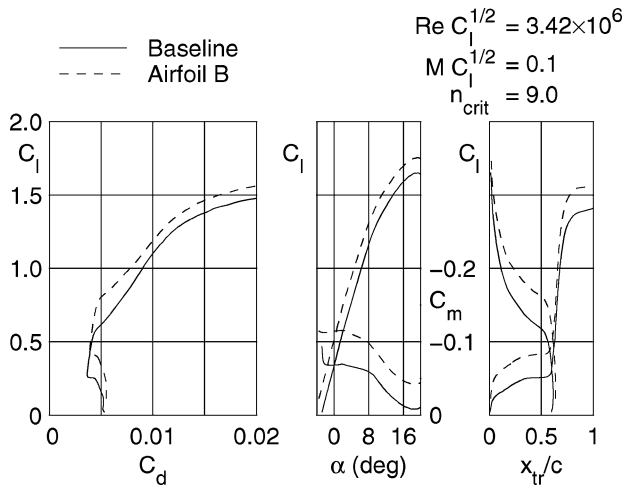

Fig. 15 Polars for the baseline airfoil and the converged airfoil B from XFOIL analysis.

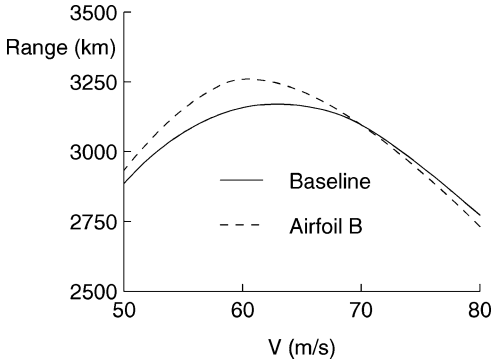

Fig. 16 Range curves with the baseline airfoil and the converged airfoil B.

that the C_l^{up} for the converged airfoil B is approximately 0.8. The variations of the aircraft range with V for the baseline and converged airfoils are shown in Fig. 16. As Fig. 16 shows, the converged airfoil B has a higher R_{max} than the baseline airfoil.

To further demonstrate that the converged airfoil B indeed has the ideal camber for maximization of range, a family of airfoils with varying camber (and, hence, varying values of C_l^{up}) were designed around airfoil B. Airfoils $B1$–$B3$ have lower camber than airfoil B, and airfoils $B4$ and $B5$ have progressively higher camber. Figure 17 shows the drag polars from XFOIL analysis for airfoils B, $B1$, and $B5$, as well as the values of C_l^{up} for the three airfoils. Figure 18 shows the variation of R_{max} as a function of C_l^{up} for this family of airfoils from postdesign analysis. As Fig. 18 shows, the R_{max} increases with

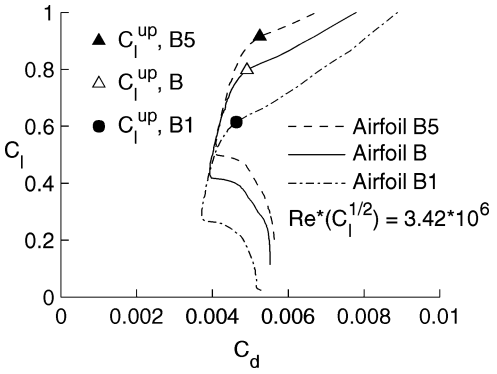

Fig. 17 Drag polars for airfoils *B*, *B*1, and *B*5.

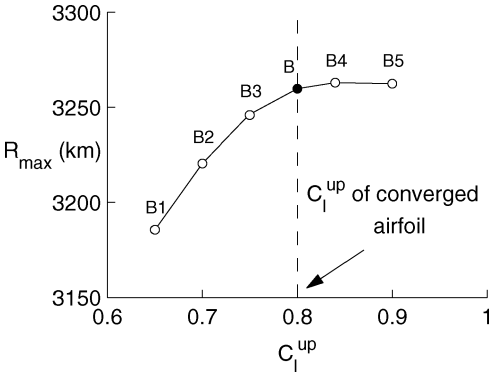

Fig. 18 Maximum range as a function of C_l^{up}.

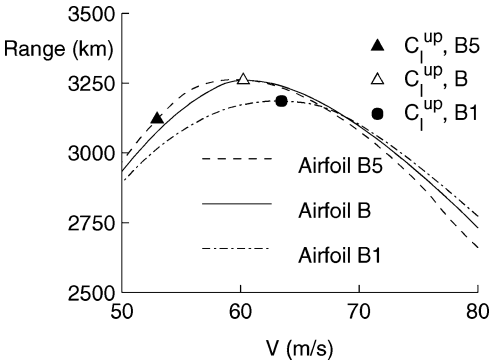

Fig. 19 Range curves with airfoils *B*, *B*1, and *B*5.

increasing C_l^{up} up to a certain value corresponding to the C_l^{up} of airfoil B. Beyond that value, further increase in C_l^{up} does not have an effect on the maximum range of the aircraft. Also note from Fig. 18 that the converged airfoil B is the ideal airfoil for R_{max}. As a further demonstration, Fig. 19 shows the range curves for airfoils B, $B1$, and $B5$. As Fig. 19 shows, airfoil $B1$ has a lower R_{max} than airfoil B and airfoil $B5$ does not have any increase in R_{max} over B. This postdesign study of the effect of C_l^{up} on R_{max} demonstrates that the design formulation is successful in identifying the ideal camber for an airfoil tailored for the R_{max} condition.

Airfoil Tailoring for R_{max} with Specified V_{stall}

As was done for the V_{max} tailoring, the tailoring for the R_{max} flight condition can also be performed with a constraint on the stall speed. When the stall speed is held constant, the wing area is adjusted at each step of the Newton iteration to account for changes to the airfoil Cl_{max}. As was observed with the V_{max} tailoring, the ideal airfoil for the R_{max} condition with a V_{stall} constraint is nearly identical to the ideal airfoil for R_{max} when the wing area was held constant. That is, airfoil B is the ideal airfoil for R_{max}, even when the stall speed is held constant.

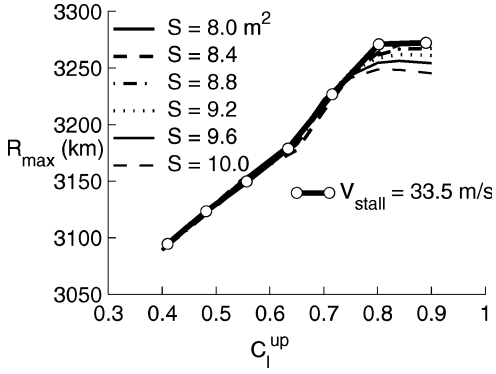

Fig. 20 R_{max} as a function of C_l^{up} for various values of S_w.

To better understand this result, a postdesign analysis study of the variation of R_{max} with C_l^{up} was performed with the B-series airfoils with different values for the wing area. The results, shown in Fig. 20, show that although the maximum range for the ideal airfoil does have a small dependence on the wing area, the ideal C_l^{up} is nearly the same for all of the wing areas considered. As seen, when V_{stall} is held constant, the value of R_{max} keeps increasing with C_l^{up} until the ideal C_l^{up} of 0.8, beyond which there is little increase in R_{max}.

Conclusions

Although there has been steady progress in the development of inverse airfoil design methods and airfoil families with specific lift, drag, and moment characteristics and geometry constraints, there has been comparatively less attention paid to tailoring an airfoil to suit an aircraft application. The design of an airfoil to maximize one or more aircraft performance parameters has traditionally required a trial-and-error process, in which the designer iterates between airfoil design and analysis and computation of the resulting aircraft performance. With an objective of shortening the airfoil–aircraft design integration time, a design formulation has been presented that incorporates aircraft performance considerations in laminar-airfoil inverse design. Two aircraft performance parameters have been considered: level-flight maximum speed and maximum range. The design problem is then posed in the form of two questions: 1) What is the ideal lift coefficient for the lower corner of the airfoil drag polar to tailor the airfoil for the aircraft level-flight maximum speed condition? 2) What is the ideal lift coefficient for the upper corner of the airfoil drag polar to tailor the airfoil for the maximum range flight condition?

The article presents a design formulation that allows for the incorporation of these design considerations in the multidimensional Newton iteration framework available in the PROFOIL inverse airfoil design code. In this Newton iteration process, the conformal-mapping variables that control the lift coefficients for the upper and lower corners of the airfoil drag bucket are automatically adjusted to tailor the airfoil for one or both of these aircraft flight conditions. As a result, the airfoil lower-surface aerodynamics are tailored so that the aircraft rate of climb is zero when the airfoil is operating at the lower corner of the LDR and likewise the airfoil upper-surface aerodynamics are tailored for the maximum-range flight condition. The method can also maintain a constant aircraft stall speed when an airfoil is tailored by adjustment of the wing area. The results of the inverse design have been validated in the article by postdesign studies that used aircraft performance computations. Although the method presented in the paper is for a piston engine-driven propeller-powered airplane, the approach can be readily extended to other types of aircraft.

The current design formulation represents a new direction in the development of inverse airfoil design methods. By the departure from the traditional effort of specification of the desired airfoil aerodynamics as input to the inverse design process, the current formulation, in addition, allows for the specification of the desired performance characteristics of the aircraft as input and the determination

of the aerodynamic specifications, as well as the airfoil geometry, as the outcome of the inverse design process.

References

[1]Mangler, W., "Die Berechnung eines Tragflugelprofiles mit Vorgeschreibener Druckverteilung," *Jahrbuch der Deutschen Luftfahrtforschung*, Vol. 1, 1940, pp. 46–53 (translated as Air Ministry of London Translation 932, 1940).

[2]Lighthill, M. J., "A New Method of Two-Dimensional Aerodynamic Design," Aeronautical Research Council R&M 2112, London, April 1945.

[3]Eppler, R., and Somers, D. M., "A Computer Program for the Design and Analysis of Low-Speed Airfoils," NASA TM 80210, Aug. 1980.

[4]Henderson, M. L., "Inverse Boundary-Layer Technique for Airfoil Design," *Advanced Technology Airfoil Research*, Vol. 1, NASA CP-2045, Pt. 1, 1978, pp. 383–397.

[5]Selig, M. S., and Maughmer, M. D., "Multipoint Inverse Airfoil Design Method Based on Conformal Mapping," *AIAA Journal*, Vol. 30, No. 5, 1992, pp. 1162–1170.

[6]Selig, M. S., and Maughmer, M. D., "Generalized Multipoint Inverse Airfoil Design," *AIAA Journal*, Vol. 30, No. 11, 1992, pp. 2618–2625.

[7]Gopalarathnam, A., and Selig, M. S., "Multipoint Inverse Method for Multielement Airfoil Design," *Journal of Aircraft*, Vol. 35, No. 3, 1998, pp. 398–404.

[8]Jepson, J. K., and Gopalarathnam, A., "Inverse Airfoil Design via Specification of the Boundary-Layer Transition Curve," AIAA Paper 2003-0212, Jan. 2003.

[9]Gopalarathnam, A., and Selig, M. S., "Low-Speed Natural-Laminar-Flow Airfoils: Case Study in Inverse Airfoil Design," *Journal of Aircraft*, Vol. 38, No. 1, 2001, pp. 57–63.

[10]Maughmer, M. D., and Somers, D. M., "Figures of Merit for Airfoil/Aircraft Design Integration," AIAA Paper 88-4416, Sept. 1988.

[11]Gopalarathnam, A., and McAvoy, C. W., "Effect of Airfoil Characteristics on Aircraft Performance," *Journal of Aircraft*, Vol. 39, No. 3, 2002, pp. 427–433.

[12]Drela, M., "XFOIL: An Analysis and Design System for Low Reynolds Number Airfoils," *Low Reynolds Number Aerodynamics*, edited by T. J. Mueller, Vol. 54, Lecture Notes in Engineering, Springer-Verlag, New York, 1989, pp. 1–12.

[13]Drela, M., and Giles, M. B., "Viscous–Inviscid Analysis of Transonic and Low Reynolds Number Airfoils," *AIAA Journal*, Vol. 25, No. 10, 1987, pp. 1347–1355.

[14]Houghton, E. L., and Carpenter, P., *Aerodynamics for Engineering Students*, Wiley, New York, 1993, pp. 373–377.